國立臺灣大學電機資訊學院資訊工程學系

碩士論文

Department of Computer Science and Information Engineering
College of Electrical Engineering and Computer Science
National Taiwan University

Master Thesis

動態乳房彈性超音波之最佳影像選取與腫瘤診斷分析

Slice Selection and Diagnosis of Dynamic Breast Elastography

徐佑維

Yu-Wei Hsu

指導教授：張瑞峰 博士

Advisor: Ruey-Feng Chang, Ph.D.

中華民國 100 年 7 月

July, 2011

國立臺灣大學碩士學位論文
口試委員會審定書

動態乳房彈性超音波之最佳影像選取與腫瘤診斷分析

Slice Selection and Diagnosis of Dynamic Breast Elastography

本論文係 徐佑維 君（學號R98922117）在國立臺灣大學資訊工程學系完成之碩士學位論文，於民國 100 年 7 月 16 日承下列考試委員審查通過及口試及格，特此證明

口試委員：張瑞峰

（指導教授）

系 主 任 呂育道

ACKNOWLEDGEMENTS

兩年的碩士生涯，在不知不覺中就已經漸漸的步入尾聲了，人生也要開始往下一步邁進，回首過去，感覺時間真的過的很快，也得到許多幫助和認識很多好朋友。

首先，第一個要感謝的就是指導教授張瑞峰老師，老師在尋找研究方向，題目的訂定，還有論文的編修和平常的學習，都會很有耐心的悉心指導，而且總是不眠不休的協助我們並且一步一步的督促我們的進度，另外也會希望我們可以自己嘗試自己解決問題，在研究和論文上也都有給予很多好的建議，而我也從中學到很多。另外，也要感謝兩位在百忙之中來參加我們的口試的口試委員，他們提供了很多寶貴的修改意見，也讓這篇論文更加的完善。

而在這兩年裡，最常見面的就是實驗室的學長姐和學弟妹還有同屆的好朋友們，雖然我們都是從不同學校進到同一間實驗室，但是這兩年的點點滴滴一定會成為我心底的一個珍貴回憶。首先，要感謝數學超強的位文，總是不嫌棄我纏著他問著一些笨問題，從他那裏我真的學到很多；另外，還有幽默的慶和，總是會說些有趣的話來讓大家開心，而且不會的問題他也不會吝於教我們；還有超聰明的戴偉，常常可以從他那學到很多，聽到很多，而和他一組做作業時，也常常會對他的創意耳目一新，而且大家總是會很好心的提醒我和教導我，不然我總是會忘東忘西的，而在碩一大家一起在實驗室念書念到凌晨，一起去問問題，一起解題，真的很讓人懷念。還要感謝人超好的毅偉，總是不嫌麻煩的幫助我們，真的是很照顧我們的給力學長，而且和球技高超的 WING 都超搞笑的，總是讓實驗室充滿歡樂，讓我們去實驗室心情都會很開心，還有 KAI 也是很威的學長，常常會幫忙解決一些很困難的問題，而且也會跟我們講很多有趣的事，另外，最要感謝的就是少謙學姊，學姐真的在我的論文修改上盡心盡力，問到不會的事也會不厭其煩的跟我解釋，另外也會跟我討論研究的問題，在最後口試的衝刺，也有一直協

助我，真的很感謝學姐的幫忙；還有愛打球的 MONKEY 學長，每個禮拜三總是會邀大家一起去打籃球，讓我們可以放鬆一下順便聊聊天，順便也可以練練我那遜遜的球技，還有耀賢學長，在論文的修改上也有幫忙我解決一些問題，不過總是會電我的魔術方塊；玉翎學姊也是一個實驗室的開心果，而且還有阿蔡，喬喬，喵喵和葡萄學弟妹，有時候也會陪我們學長聊聊天，玩玩遊戲，還會一起討論一些問題，也讓實驗室更加的歡樂，最後也要感謝 buddy，醫生，榮泰跟鴻豪學長，實驗室就是因為有大家，所以才會充滿著歡樂，這兩年真的讓我覺得很開心也很依依不捨。

最後，也要感謝我的爸爸，媽媽和我的哥哥，他們在我難過的時候會給我安慰和支持，在我壓力大的時候也會給我鼓勵，因為有你們的支持，我才能在順利的在這條路上走下去，真的很感謝你們不求回報的默默支持著我，而我的人生也將要往下一個階段前進，希望我可以努力的進步，朝著我的夢想前進，也祝福我們實驗室大家的感情都不會隨著時間變淡，希望我們的友情會一直存在，願在這段時間不辭辛苦幫助我的人們，可以每天都開開心心，身體健康，事事順利。

動態乳房彈性超音波之最佳影像選取與腫瘤診斷分析

研究生：徐佑維　　指導教授：張瑞峰　博士

國立台灣大學資訊工程研究所

摘要

乳癌一直是全球婦女的主要死因之一，而且良性和惡性腫瘤間的不同硬度已經被醫生視為在觸診的重要特徵。近年來，乳房彈性超音波已經被使用來評估病人腫瘤的彈性程度，醫生需要對腫瘤組織施與輕微的壓力以便取得一段動態彈性視訊，而軟硬資訊則根據腫瘤組織的位移得到，另外，因為健康的組織和患病的組織有不同的軟硬程度，所以由乳房彈性超音波取得的彈性資訊已經被證明對於區分良惡性腫瘤是有幫助的，診斷時醫生將會從視訊中選出一張具有代表性的影像進行腫瘤分析。此篇論文的目的是利用提出的自動選圖方法選出一張影像並且針對這張影像來擷取特徵去診斷腫瘤。首先，為了減少不同醫生的主觀性選圖的影響，我們會利用我們提出的自動選圖方法來選出一張最具代表性的彈性影像。接著，會使用 Level Set 方法來自動地切割出腫瘤輪廓，而不是藉由醫生來手動圈選出腫瘤以保持切割結果的一致性。最後，我們會藉由腫瘤輪廓來擷取彈性特徵去診斷腫瘤。本實驗中以 80 個經過病理驗證的病例進行測試，包含 45 個良性以及 35 個惡性的病例，並且比較自動選圖方法所選影像和醫生選影像的診斷結果。經由實驗可以得知，我們提出的選圖方法的準確率為 71.25%，靈敏度為 91.43%，

專一性則為 55.56%;然而，當使用醫生選圖時，準確率只有為 65.00%，靈敏度為 77.14%，專一性則為 55.56%。雖然自動選圖的靈敏度和準確率比醫生選圖好，但根據實驗結果統計分析，二者尚未具有統計上的差異。不過因自動選圖方法和醫生選圖在統計上是有相近的診斷結果，所以我們提出的自動選圖方法是可以幫助醫生選出具有代表性的影像以減少醫生選圖的時間。

關鍵詞： 彈性超音波、乳房腫瘤、腫瘤切割、代表性影像、電腦輔助診斷。

Slice Selection and Diagnosis of Dynamic Breast Elastography

STUDENT: YU-WEI HSU
ADVISOR: DR. RUEY-FENG CHANG

INSTITUTE OF COMPUTER SCIENCE AND INFORMATION ENGINEERING
NATIONAL TAIWAN UNIVERSITY

Abstract

The breast cancer is always the main causes of death for women and different firmness of benign and malignant tumors has been treated as an important characteristic by physicians during breast palpation. In recent years, the sonoelastography has been applied to evaluate the tumor strain of patient in clinical diagnosis. The physicians need to slightly press the tumor to obtain the dynamic elastographic image sequences. The tumor strain will be acquired on elastography based on the displacement of the tumor. Because the healthy and diseased tissues have different strain information, the elasticity information provided by the elastographic image in sonoelastography video has been proved to be useful in differentiating benign and malignant tumors. The physicians will select a representative slice from the dynamic elastographic image sequences to diagnose the tumor. In this study, the main purpose is to develop an automatic slice-selection method to select the representative slice from the sonoelastography video and then to diagnose the tumor by means of the elastographic features generated from the selected slice. Firstly, the representative slice is automatically selected by the proposed slice-selection method in order to reduce the

selection variability of physicians. Then, the contour of tumor segmented by the physicians is substituted with an automatic segmentation of level set method so as to improve the consistency of the segmentation between the different operators. Finally, the contour of tumor is used to compute the elastographic features for diagnosing the breast tumor. This study has collected 80 biopsy-proved breast tumors comprised of 45 benign and 35 malignant lesions to estimate the performance of the slice-selection method. The representative slice chosen by the proposed scheme will be compared with the physician-selected slice. The experiment shows that the diagnosis performances of accuracy, sensitivity, and specificity evaluated by the leave-one-out method based on the elastographic features for the representative slice selected by the proposed slice-selection method are 71.25%, 91.43% and 55.56%, whereas 65.00%, 77.14% and 55.56% for the physician-selected slice. That is, the sensitivity and accuracy of proposed slice-selection method is better than physician-selected slice and the specificity of these two different schemes is similar. According to the statistical analysis of experimental result, the performance of the proposed slice-selection method is similar with that of the physician's selection. Therefore, the proposed slice-selection method could assist the physician in selecting the appropriate representative slice and decreasing the time of selection.

Keywords：sonoelastography, breast tumor, tumor segmentation, representative slice.

TABLE OF CONTENTS

LIST OF FIGURES

LIST OF TABLES

Chapter 1

Introduction

Different firmness of benign and malignant tumors has been treated as an important characteristic by physicians during breast palpation [1]. The stiffer and less mobile tumors are more likely considered as malignant ones. A dynamic ultrasound imaging technique named elastography measures the degree of deformation under pressure to estimate tissue stiffness [2, 3]. It was proved that the elasticity information provided by the strain image in elatography is helpful in differentiating benign and malignant tumors [1, 4-6] since healthy and diseased tissues have different strain information.

Area ratio [1, 2, 4, 7] and elasticity score [7-9] are two popular criteria adopted by physicians on interpreting ultrasound elastography. Area ratio refers to the ratio which the tumor area on the strain image divided by the tumor area on the conventional B-mode image. And elasticity score was classified into grade 1 to grade 5 according to the distribution of tissue strain within the tumor. These two generally used criteria were compared in [7] and concluded that the area ratio performed better than the elasticity score in classifying benign and malignant tumors. In addition, some researches focused on comparing the diagnostic performance of the conventional ultrasound and elastography. Most of these studies [7, 10-13] have made a conclusion that conventional ultrasound has higher sensitivity and the elastography has higher specificity in tumor diagnosing.

Since there are multiple slices in each dynamic elastographic video, physicians need to select the most appropriate slice for diagnosing tumors captured in the scanned video. Some studies had reported that diagnosing based on elastography is dependent

on inter-observer variability and influenced by the image quality [6, 14]. Chang et al. [15] proposed a scheme to assess the qualities of elasticity images and classified into three categories. They had showed there are significant difference between the sensitivities of higher-quality and lower-quality images (87.0% vs 56.8%) in diagnosing tumors. Moreover, our previously proposed study [16] provided a fair breast tumor diagnostic system but also suffered from the same problem in slice selection. Therefore, to reduce the influences of different image qualities and to provide a stable diagnostic performance, we had developed a representative slice selection technique to objectively choose the image with the best quality from each scanned elastographic video. The representative slice of each video was selected based on the distribution of tissue strain within whole strain image. Moreover, the level set technique was applied on B-mode image to automatically segment tumor and avoid the variability of manually determining tumor contours between different radiologists. Finally, some quantitative features were extracted from the elasticity information within the segmented tumor region for the following tumor diagnosis.

Chapter 2

Materials

2.1 Elastographic image

The elastographic US in this study was scanned by an experienced radiologist of breast ultrasound using Siemens ACUSON S2000 Ultrasound System (Siemens Medical Solution, Malvern, PA, USA) with a 5-14 MHz linear transducer. Each of our scanned elastography was saved in DICOM format, which includes at least 50 images. Fig. 1 illustrated the standard elastographic image captured using ACUSON S2000. Each image contains both B-mode (left side) and elastographic (right side) US of the target tumor. The elastographic image depicted tumor strain is displayed in a 256-grayscale image, where gray-level 0 represents the hardest tissue and 255 the softest tissue. For each elastography sequence, we had developed an image selection technique to choose the most appropriate image for tumor diagnosis.

2.2 Lesions

This study had collected informed consents from patients and was approved by the local ethics committee. The experimental elastography of 80 breast tumors (45 benign and 35 malignant) in 80 women (age range from 19 to 79 years, mean 49.7±11.34 years) were collected from December 2009 to December 2010. There were 29 cases of invasive ductal carcinoma, and 6 cases of ductal carcinoma in situ (DCIS) in malignant tumors. In addition, there were 36 cases of fibrocystic changes (including ductal hyperplasia, sclerosing adenosis and fibroadenomatous change), 2 cases of atypical ductal hyperplasia, 5 cases of papillomas, 2 cases of fibroadenomas, in benign tumors. The tumor size measured at the B-mode US was 4-9.7 mm in 27 lesions,

10-14.3 mm in 31 lesions, 15-19.4 mm in 15 lesions and 20-57 mm in 7 lesions. Moreover, the sizes of lesions were 4-31 mm (mean, 11.88±5.66 mm) for fibrocystic changes, 9-11 mm (mean, 9.62±0.88 mm) for papillomas, 12-18 mm (mean, 15±4.24 mm) for fibroadenomas, 6-13.6 mm (mean, 9.8±5.37 mm) for atypical ductal hyperplasia, 5-57 mm (mean, 14.69±9.49 mm) for invasive ductal carcinoma and 8-19 mm (mean, 13.17±4.36 mm) for DCIS.

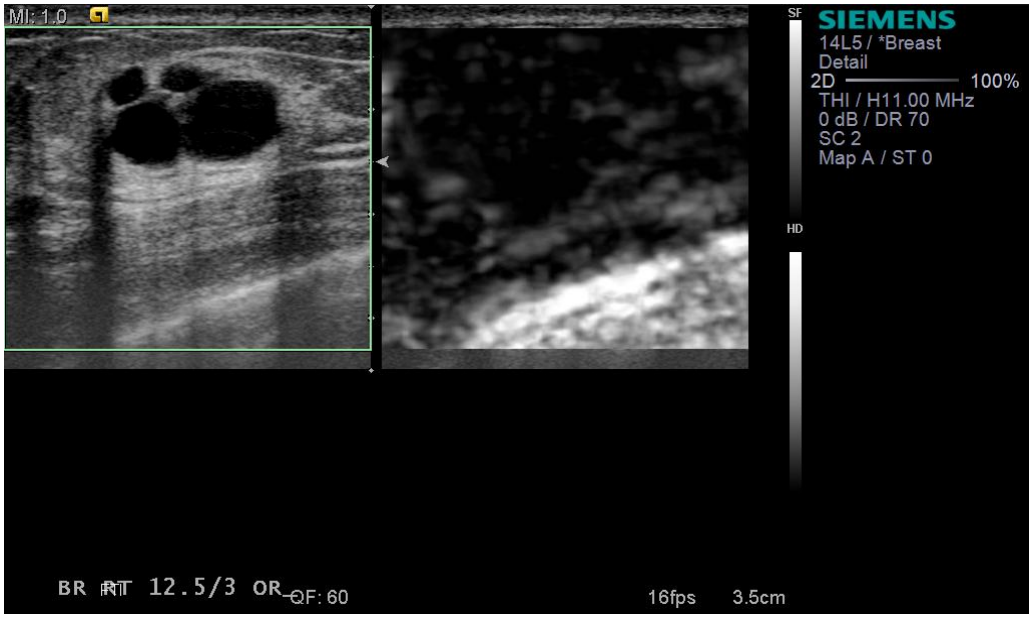

Fig. 1 The elastographic image.

Chapter 3

The Proposed Method

In the dynamic elastographic image, there are several 2-D slices and a representative slice should be selected for further diagnosis. Due to the different compression applied for each slice, the stiffness ratio in each slice is different. In this study, the stiffness ratio of each slice will be computed and sorted in the ascending order and the slice ranking at appropriate percentile will be selected. Then, the tumor segmentation method is applied for the selected representative slice to delineate the tumor contour based on the B-mode part of elastographic slice. Finally, by utilizing the elasticity information in the tumor region which is found in the B-mode part, the tumor stiffness ratio and other elastographic features could be evaluated. The flow chart of the proposed system is shown in Fig. 2.

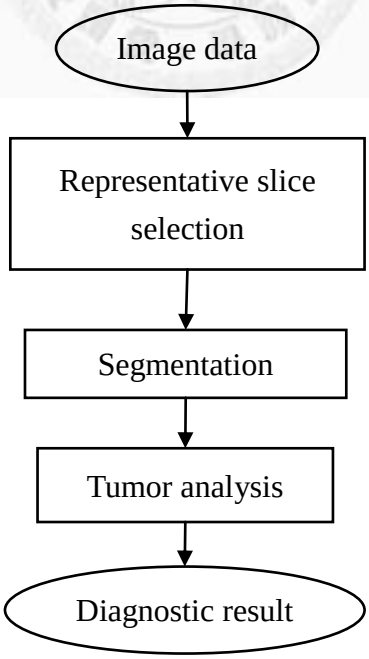

Fig. 2 Flow chart of the proposed system.

3.1 Representative Elastographic Slice

Before diagnosing the tumor, a representative slice will be selected automatically by the proposed system from the dynamic elastographic image. At first, the stiffness ratio is computed based on the elasticity information of each slice. Next, these stiffness ratios are sorted in the ascending order and then the representative slice is chosen based on their ranking of stiffness ratios. In order to decide the better representative slice, the slices ranking at different percentile will be used for comparison in the experiment.

3.1.1 Slice Selection Method

Because of different pressure applied on the tumor during scanning process, the elasticity information of each slice may be different. In this study, we developed a slice selection method to eliminate the influence of nonuniform stress in the scanned video. The stiffness ratio is applied to evaluate the degree of pressure and one slice with appropriate elasticity will be selected as the representative slice.

At first, a threshold value TH_{slice_stiff} is used to decide whether a pixel is stiff or not. A better threshold value between 10 and 30 will be decided by experiments. After classifying the pixels into stiff or soft, the stiffness ratio of the whole elastographic image could be computed by the number of stiff pixels divided by the total number of pixels. Next, the stiffness ratio of each slice will be sorted in the ascending order. At last, the slices at the 25^{th}, 50^{th}, and 75^{th} percentile will be selected, as shown in Fig. 3. To avoid selecting the incorrect over-compressed or under-compressed slices, the slice at the 0^{th} (lowest strain) and 100^{th} (highest strain) percentile will be abandoned. Furthermore, the representative slice is chosen from the above mentioned three slices with the most appropriate slice with enough and stable pressure. Actually, the threshold

value TH_{slice_stiff} will affect the selection of the above possible three slices. If a low threshold value is used then the slice at low percentile will be selected. The different combination of threshold values and percentiles will be tested at experiments.

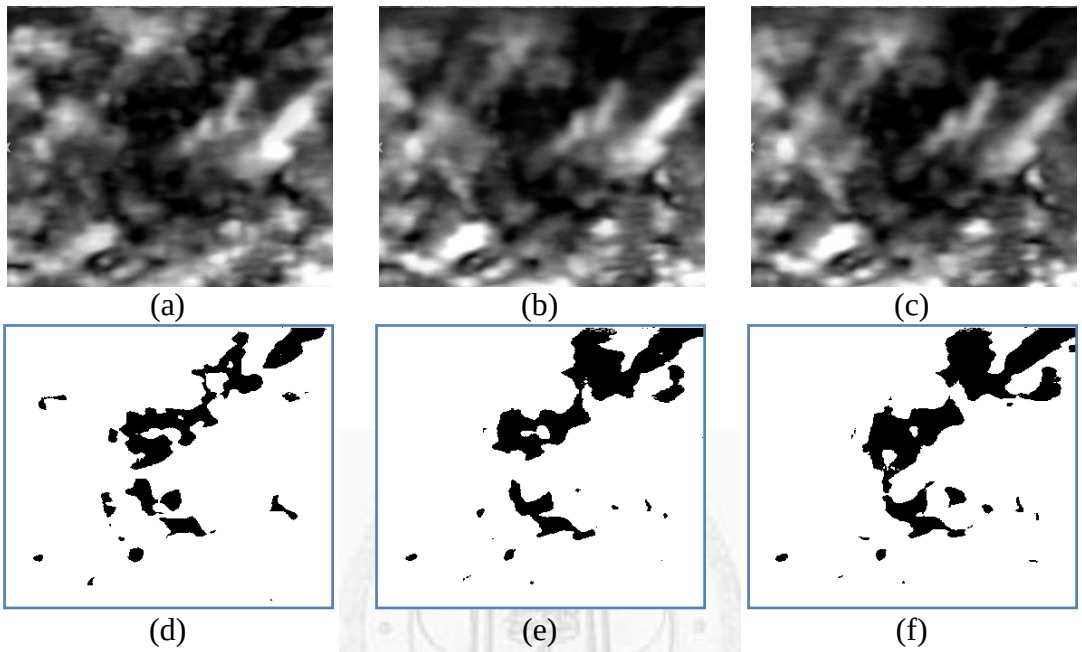

Fig. 3 Examples of elastographic image with (a) the 25th percentile and (b) the 50th percentile and (c) the 75th percentile after sorting in the ascending order. (d)-(f) The produced binary image of (a)-(c) after thresholded with value 15.

3.2 Segmentation

After selecting the representative slice, in order to evaluate the tumor features for diagnosis, the contour of tumor should be delineated first. In this paper, the tumor contour will be segmented by means of the level set method [17, 18] after a series of preprocessing.

At first, the sigmoid filter [19] is applied to enhance the contrast of the original B-mode part so as to increase the distinction between tumor and background. Then, in order to get the information of edge, the gradient magnitude filter [20] will be utilized

to obtain the gradient image. Moreover, the sigmoid filter will be employed again to enhance the contrast of gradient image for the better result. Finally, the contour of tumor in the B-mode part will be segmented by the level set method. In addition, in order to eliminate the holes in the tumor and smooth the contour, the morphology closing operation [21-24] will be applied to the image produced by the level set method. The flowchart of the segmentation is illustrated in Fig. 4.

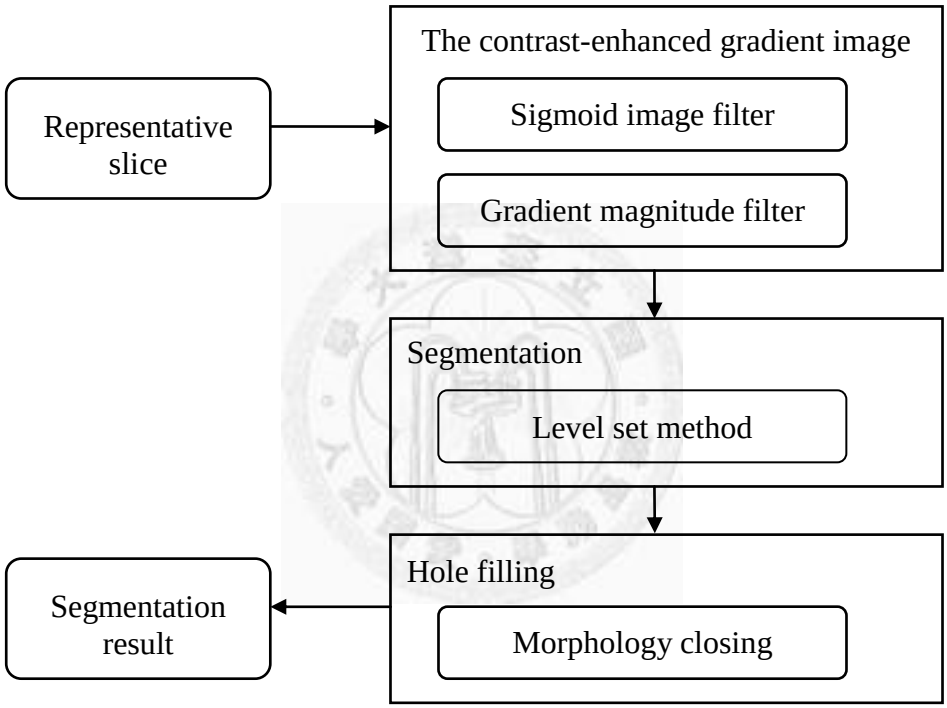

Fig. 4 Flow chart of the segmentation method

3.2.1 The Contrast-enhanced Gradient Image

Actually, the result of segmentation will be not good if the level set method is directly utilized on the B-mode part of the original elastographic image. Therefore, the sigmoid filter is needed to enhance the contrast of image and the gradient magnitude filter is also required for obtaining the information of edge. Furthermore, the resulted image produced by the sigmoid filter and gradient magnitude filter will be treated as

the input of the level set method. These two methods will be introduced in the following section.

3.2.1.1 Sigmoid image filter

Even though the level set method is applied to the image generated by the gradient magnitude filter, the result will still be not good because of the speckle noise appeared in the B-mode image. Therefore, the sigmoid filter will be utilized to enhance the contrast of image for preserving just the significant edge information in the resulted image of the gradient magnitude filter. The sigmoid function is defined as

$$I' = (Max - Min) \cdot \frac{1}{\left(1 + e^{-\left(\frac{I-\beta}{\alpha}\right)}\right)} + Min \qquad (1)$$

where I is the input intensity of the original image, I' is the output intensity, *Max* and *Min* are the maximum and minimum intensity values of output image, α is the width of the intensity window, and β whose value is equal to *Min* in this paper is the center of the intensity window. The initial seeds chosen by the user for segmenting the tumor will be used to evaluate α automatically. That is, the circle around each seed with radius of 10 pixels is applied to compute the mean of seed neighborhood and α is represented as the maximum of the mean of seed neighborhood. Moreover, the pixels whose intensity is higher than α in the background are set to *Max* and the distinction of intensities between the tumor and background will be more manifest by means of utilizing α and β. Further, the level set method can march faster on the homogeneous regions with the help of the image whose contrast has been enhanced. The result of sigmoid filter on the B-mode part of the original elastographic image Fig. 5(a) is exhibited in Fig. 5(b).

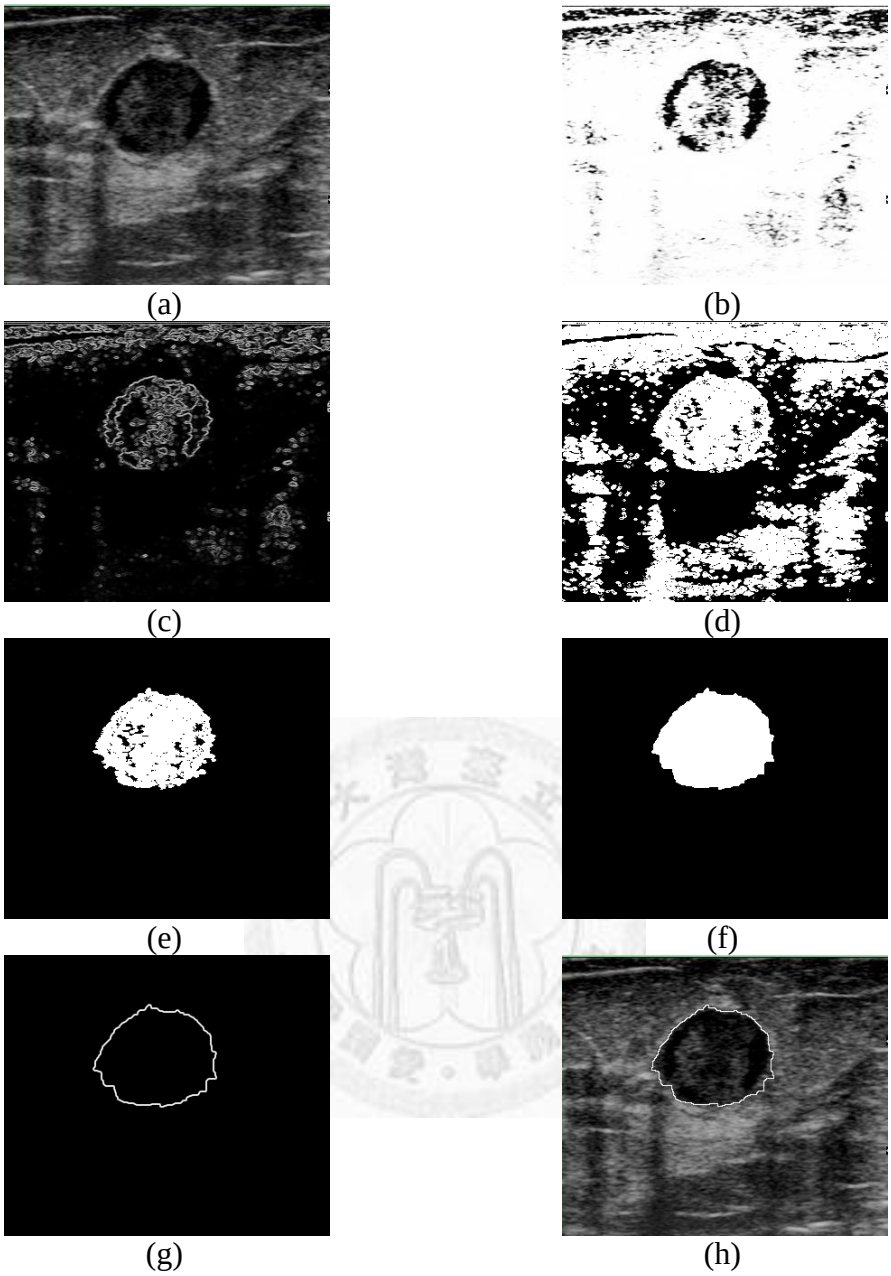

Fig. 5 Step-by-step illustration of automatic tumor segmentation. (a) Original B-mode image (b) Utilizing the sigmoid filter with α=7, β=0, min=0, and max=255 (c) Gradient magnitude filter (d) Utilizing the sigmoid filter with α=0.01, β=0.5, min=0, and max=255 (e) Applying the level set method before the morphology closing operation (f) Morphology closing operation (g) The determined tumor contour (h) Overlapping tumor contour onto the original B-mode image.

3.2.1.2 Gradient magnitude filter

In this section, the gradient magnitude filter is utilized to find the information of edge and segregate one uniform region from the other different regions so as to detect the contour of tumor and promote level set segmentation to get a better result. For the image $I(x, y)$, its gradient $\nabla I(x, y)$ is represented as [24]

$$\nabla I(x, y) = \begin{bmatrix} g_x \\ g_y \end{bmatrix} = \begin{bmatrix} \frac{\partial I}{\partial x} \\ \frac{\partial I}{\partial y} \end{bmatrix} \tag{2}$$

The magnitude of gradient $\nabla I(x, y)$ is defined as

$$mag(\nabla I) = \sqrt{g_x^2 + g_y^2} \tag{3}$$

Moreover, in order to evaluate the g_x and g_y, two gradient magnitude masks will be applied to convolve image, as shown in Fig. 6. In addition, it is noted that sigmoid filter will be utilized again to enhance the contrast of the result image produced by the gradient magnitude filter for the better result of the segmentation. The gradient magnitude image for Fig. 5(b), which is enhanced again by sigmoid filtering, is represented as Fig. 5(c), and the contrast-enhanced gradient magnitude for Fig. 5(c) is shown in Fig. 5(d).

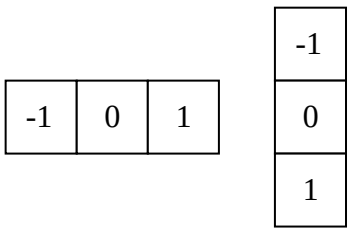

Fig. 6 The gradient masks (a) g_x and (b) g_y.

3.2.2 Level Set Method

The level set method is a common numerical technique which is easy to model complicated shape. It will maintain robust and accurate even during tracking interfaces with complex motions. The purpose of level set method is to track the evolving contour; therefore it is adopted for segmenting tumor in this paper. Moreover, the features of image such as edge and gradient are utilized to help the level set method to evaluate the result of segmentation.

First, the user choose multiple seeds regarding as the initial contour $\gamma(t)$ embedded as the zero level set of a higher dimensional level-set function $\psi(x, t)$, where the zero level set is defined as $\Gamma(x, t) = \{\psi(x, t) = 0\}$ and x is a point in $\Re^N$. Then, the partial differential equation is applied to the level-set function for evolving the initial contour. For the initial contour $\gamma(t=0)$, the level-set function is defined as

$$\psi(x, t=0) = \pm d \tag{4}$$

where d is the distance from x to $\gamma(t=0)$, and the sign is represented as a point which is outside of or inside of the initial contour corresponding to a positive or negative value, as illustrated in Fig. 7.

Furthermore, because of providing the velocity in the outward normal direction by F and the partial differential equation for ψ has been evaluated, the level-set function is represented as [18, 25]

$$\psi_t + F|\nabla\psi| = 0 \tag{5}$$

with a given value of $\psi(x, t=0)$. The result image generated by level set method for Fig. 5(d) is exhibited in Fig. 5(e), and the contour of the final result overlapping with the original B-mode part of the elastographic image is depicted in Fig. 5(h).

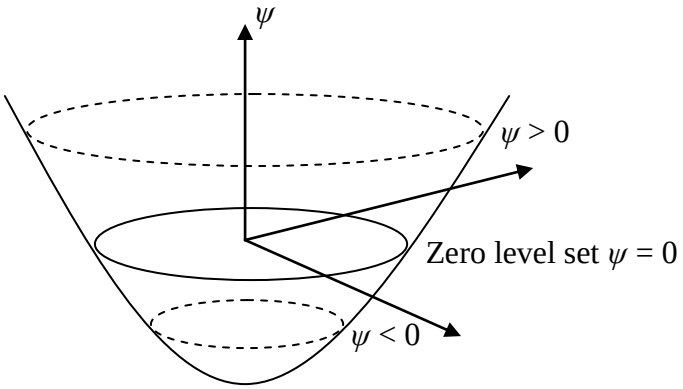

Fig. 7 The zero set in a level set. The sign of $\psi(x, y, t)$ is decided by whether the position of the point is inside the zero level set (negative) or outside the zero level set (positive).

3.2.3 Morphology Closing Operation for Hole Filling

After tumor segmentation, one more technique is needed for solving some defects. Because of some small holes will exist inside of the tumor in the image produced by the level set method, the mathematical morphology closing operation with 5×5 ball structuring element is applied to deal with the problem and smooth the contour of tumor. The result of the morphology closing operation is illustrated in Fig. 5(f).

3.3 Elastographic Feature Analysis

After segmenting the contour of tumor by the level set method from the B-mode image, the contour will be applied to the elastographic image in order to extract tumor features, as shown in Fig. 8. By means of analyzing elasticity information inside the segmented tumor and its neighborhood region, the computed elastographic features can be utilized to diagnose the tumor. Moreover, the features can be divided into five classes: stiffness ratio, average intensity of center box, tumor boundary elasticity, outside-tumor elasticity, inside-tumor elasticity. In this section, the elasticity information is represented as grayscale intensity.

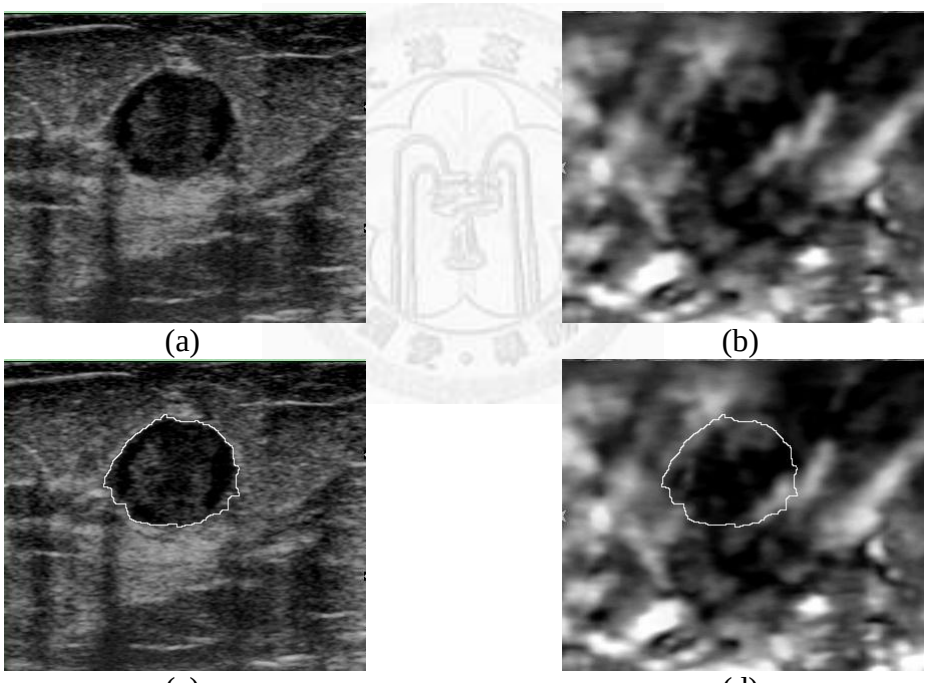

Fig. 8 The processed images (a) original B-mode US image (b) original elastographic image (c) the contour of tumor delineated on the B-mode US image (d) the contour of tumor overlapped with the elastographic image.

3.3.1 Stiffness Ratio

In the elastographic image, the stiffness of tumor can be represented as the ratio of the dark pixels inside tumor. The stiffness ratio has been proven to be a significant diagnostic feature in [8], therefore the stiffness ratio will be utilized in this paper. Two schemes including thresholding and fuzzy c-means (FCM) [26] were used to classify pixels within the segmented tumor to compute stiffness ratio represented as

$$stiffness\_ratio = \frac{stiff\_num}{total\_num} \tag{6}$$

where the *stiff_num* means the number of the stiff pixels in the tumor and the *total_num* stands for the total number of pixels in the tumor. In the thresholding scheme, pixels within tumor were classified into two groups using the predefined threshold $TH_{stiffness}$. Since we tried to figure out the best threshold value, different $TH_{stiffness}$ values (5, 10, 15, 20, 25, 30, 40, and 50) were used in our experiments and the corresponding stiffness ratios were defined as $stiff_5$, $stiff_{10}$, $stiff_{15}$, $stiff_{20}$, $stiff_{25}$, $stiff_{30}$, $stiff_{40}$, $stiff_{50}$. In the fuzzy c-means scheme, pixels within a tumor were classified into two or three categories and two stiffness ratios *fcm2_ratio* and *fcm3_ratio* were defined as the ratio of pixels in the stiffest group to all tumor pixels. In addition, the stiffest group of the two and three classes classified by the fuzzy c-means method will also be applied to evaluate the stiffness mean which can represented as the averaging gray intensity of pixels in the stiffest group. The stiffness mean is defined as

$$stiffness\_mean = \frac{1}{N_{stiff}} \sum_{p \in stiff} I(p) \tag{7}$$

where $I(p)$ is the gray intensity of the pixel p, and N_{stiff} is the number of the stiff pixels in the tumor.

3.3.2 Average intensity of center box

The 20×20 and 30×30 boxes at the center of the tumor will be defined firstly, as shown in Fig. 9 Then the average of pixel intensities in these two boxes will be computed to analyze the tumor. These two box features are defined as

$$avg\_box_{20} = \frac{1}{N_{box20}} \sum_{p \in box20} I(p) \quad \text{and} \tag{8}$$

$$avg\_box_{30} = \frac{1}{N_{box30}} \sum_{p \in box30} I(p) \tag{9}$$

where $I(p)$ denotes the gray intensity of pixel p, and N_{box20} and N_{box30} are the number of pixels in the 20×20 and 30×30 boxes, respectively.

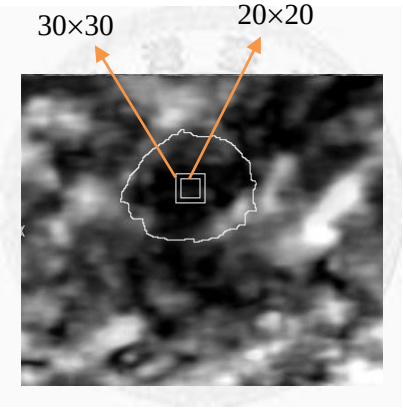

Fig. 9 The 20×20 and 30×30 boxes at the center of the tumor.

3.3.3 Tumor boundary elasticity

The morphological dilation and erosion operation with a 10×10 ball structuring element will be utilized to define the outer and inner bands around the contour of tumor, as shown in Fig. 10. The average gray intensities of pixels in these two bands will be calculated as two features for diagnosing the tumor. The definitions of these two features are

$$inner\_mean = \frac{1}{N_{inner}} \sum_{p \in inner} I(p) \quad \text{and} \tag{10}$$

$$outer\_mean = \frac{1}{N_{outer}} \sum_{p \in outer} I(p) \tag{11}$$

where the $I(p)$ denotes the gray intensity of pixel p, and N_{inner} and N_{outer} the number of pixels in the inner or outer bands around the contour of tumor. Furthermore, the elastic difference between the inner and outer bands is also applied as a diagnostic feature. The elastic difference of two bands is defined as

$$diff\_bands = outer\_mean - inner\_mean \tag{12}$$

In addition, the average gray intensity of the entire tumor which can stand for the average elasticity of the tumor is used as a feature as well. The mean feature is represented as

$$tumor\_mean = \frac{1}{N_{tumor}} \sum_{p \in tumor} I(p) \tag{13}$$

where $I(p)$ is the gray intensity of the pixel p and N_{tumor} denotes the number of pixels inside of the tumor.

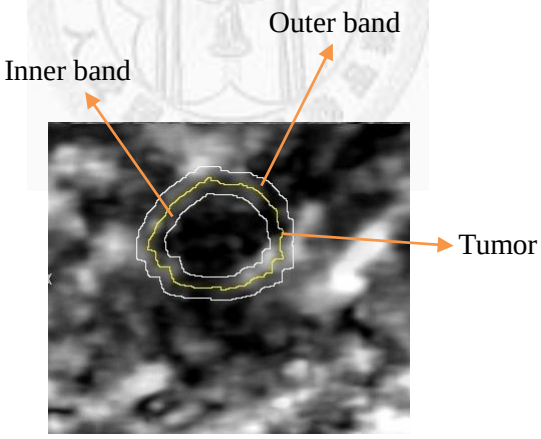

Fig. 10 The inner and outer bands with morphology dilation and erosion operation with 10×10 ball structuring element.

3.3.4 Outside-tumor elasticity

As previously mentioned in section 3.3.3, the morphological dilation operation with 10×10 ball structuring element was firstly applied to indicate the outer regions

around the contour of tumor. Then the outer-tumor region was partitioned into eight different regions, named Left (L), Right (R), Up (U), Down (D), UpperLeft (UL), UpperRight (UR), LowerLeft (LL), LowerRight (LR), according to the gravity center of the tumor. The eight partitioned regions were regarded as the features to analyze the elasticity information, as shown in Fig. 11. The elasticity information of these regions will be evaluated as

$$avg\_outer\_region_i = \frac{1}{N_i}\sum_{p\in i} I(p), i \in \{L, R, U, D, UL, UR, LL, LR\} \quad (14)$$

where $I(p)$ represents the gray intensity of pixel p, and N_i means the number of pixels in the eight different regions defined above. Furthermore, the minimum value and the average value of the four regions, Up, Down, Right, and Left, were also be computed as

$$min\_outer = \min(avg\_outer\_region_i), i \in \{L, R, U, D\} \quad (15)$$

$$avg\_outer = \frac{1}{4}\sum_i avg\_outer\_region_i, i \in \{L, R, U, D\} \quad (16)$$

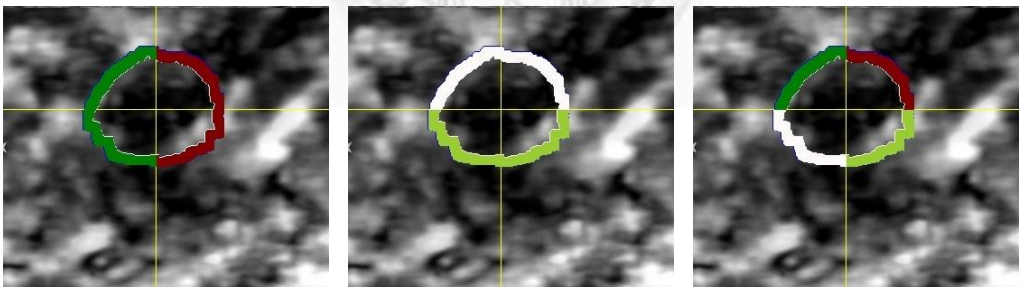

(a) (b) (c)

Fig. 11 The eight different outer regions which are at the (a) Left, Right, (b) Up, Down, (c) UpperLeft, UpperRight, LowerLeft, and LowerRight.

3.3.5 Inside-tumor elasticity

In order to evaluate the diagnostic performance of features extracted in different positions of the tumor, the elasticity within five distinct squares inside the tumor will be

utilized as the features. At first, the gravity center and the bounding box of the tumor were computed. Next, four lines were plotted at center positions between the gravity center and the bounding box, forming four rectangles, rec_{UL}, rec_{UR}, rec_{LL}, rec_{LR}, around the tumor gravity center, rec_C. Furthermore, four line segments were plotted at the center positions between previously mentioned four lines and the tumor gravity center, forming one rectangle centered at the tumor gravity center, as shown in Fig. 12. The average gray intensity of these five rectangles was calculated as the features for diagnosing the tumor. The rectangle features were defined as

$$avg\_inner\_region_i = \frac{1}{N_i}\sum_{p\in i} I(p), i \in \{rec_{UL}, rec_{UR}, rec_{LL}, rec_{LR}, rec_c\} \quad (17)$$

where $I(p)$ is the gray intensity of the pixel p, and N_i denotes the number of pixels in aforementioned different rectangles. In addition, the average and the minimum intensity of the five rectangles were also regarded as features to evaluate the elasticity information. These two features are defined as

$$min\_inner = \min(avg\_inner\_region_i), i \in \{rec_{UL}, rec_{UR}, rec_{LL}, rec_{LR}, rec_c\} \quad (18)$$

$$avg\_inner = \frac{1}{5}\sum_i avg\_inner\_region_i, i \in \{rec_{UL}, rec_{UR}, rec_{LL}, rec_{LR}, rec_c\} \quad (19)$$

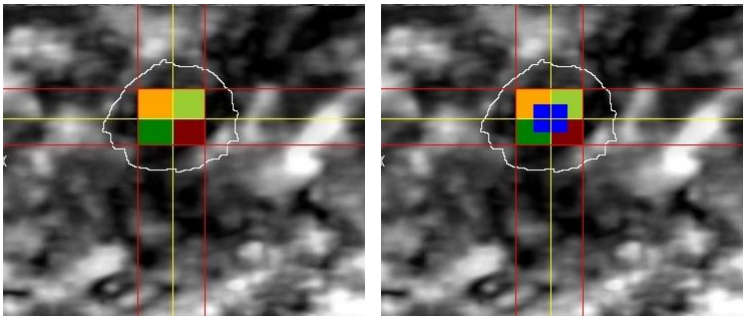

(a) (b)

Fig. 12 The five different rectangles (a) four of them around the tumor gravity center (b) one at the tumor gravity center.

Chapter 4

Experiment results

In the following experiments, the features of the elastographic image will be extracted from both our selected representative slice and physician selected slice to compare their diagnostic performance. At first, the representative elastographic slice is selected from the dynamic elatographic image automatically by means of the proposed slice-selection method. Then, the tumor contour delineated from the B-mode image by the proposed segmentation method is applied to the elastographic image. The elasticity information acquired from the tumor region in elastographic image was regarded as the tumor features and used to evaluate the performance of diagnosis. Furthermore, the performances of representative slices selected using different threshold values (TH_{slice_stiff} mentioned before) and different sorting percentiles applied on both whole image and tumor region were compared in order to obtain the most appropriate slice, as listed in Table 1. At last, the most appropriate slice chosen by our method was compared with the physician-selected slice based on their diagnostic performance of tumor in the experiment.

The binary logistic regression model [27, 28] is applied to analyze the elastographic features so as to classify the tumor into benign and malignant. The predicted values generated by the binary logistic regression model range from 0 to 1. For determining the most appropriate threshold value applied on the predicted values, we had tried different thresholds for classifying tumors and the corresponding performance measures were listed in Table 2. The probability threshold was finally set as 0.175 since it resulted in the best accuracy and superior sensitivity. After deciding the diagnostic threshold, each tumor was classified as malignant if its predicted value

was larger than or equal to the threshold, otherwise benign. In addition, the leave-one-out cross-validation method [29] is utilized to fairly evaluate the diagnostic performance of our proposed scheme. The method will choose one case as the test set and the rest of cases are deemed as training set. Then, the results of all the cases which each case has been employed as the test set in a repeated process will be merged.

The proposed system is implemented by the programming language C++ under the Microsoft Visual C++ 2005 (Microsoft, Redmond, WA, USA), operating with Microsoft Windows XP operating system (Microsoft, Redmond, WA, USA), and running on the Intel Pentium (2.67G Quad-core machine with 2.99 GB RAM).

4.1 Statistical Analysis

Since there were lots of elastographic features proposed in our study, we had to figure out which features are helpful in classifying tumors. In the beginning, the Kolmogorov-Smirnov test [30] was applied on each proposed elastographic feature to test if it is normally distributed. Once the feature is normally distributed, we calculate its mean and standard deviation corresponding to benign and malignant tumors and furthermore utilized the Student's t-test [30] to determine if this feature is sufficient to distinguish benign and malignant tumors. On the other hand, the Mann-Whitney U test [30] is applied on those non-normally distributed features to estimate if they could be used to clearly classify tumors into benign and malignant. The statistical significance level of both the Student's t-test and the Mann-Whitney U test were set to 0.05.

After determining useful features in identifying tumor pathology, the binary logistic regression model were applied on those features generating predicted values between 0 and 1. The generated predicted values were used to classify tumors. The indicators for assessing the performance are accuracy, sensitivity, specificity, positive

predictive value (PPV) and negative predictive value (NPV). Moreover, the receiver operating characteristic (ROC) curve was plotted using the ROCKIT software (C. Metz; University of Chicago, Chicago, IL, USA) and the areas under the ROC curve (Az) are also regarded as the performance indicator. Furthermore, the chi-square test [30] is utilized to evaluate the performance comparison between two different schemes. The *p*-value less than 0.05 for each comparison means a statistically significant difference. The statistical analysis except the ROC curve analysis and the binary logistic regression is conducted by the software (SPSS, version 16 for Windows; SPSS, Chicago, IL, USA).

4.2 Elastographic features analysis

Because not all the features are beneficial for diagnosing the tumor, the mean value, standard deviation (SD), median value, and the *p*-value generated from the Student's t-test or Mann-Whitney U test will be applied to evaluate the statistically significant difference of the features in order to choose the more useful features. Then, the different values including the mean value, standard deviation (SD), median value and the *p*-value of the Student's t-test and Mann-Whitney U test based on the features corresponding to the malignant and benign cases on the slice-selection method with TH_{slice_stiff} = 15 and at the 25^{th} percentile and the physician-selected slice were listed in Table 3 and Table 4, respectively.

Table 1 The Az values of ROC analysis applied on tumor region and whole slice with different threshold values TH_{slice_stiff} and different percentiles.

	Tumor region					Whole slice				
TH_{slice_stiff} / Percentile	10	15	20	25	30	10	15	20	25	30
25^{th}	0.5937	0.6610	0.7200	0.7479	0.7854	0.7219	0.8019	0.6883	0.7200	0.7797
50^{th}	0.6984	0.7194	0.6533	0.7384	0.7416	0.6533	0.6902	0.6667	0.7746	0.6711
75^{th}	0.6724	0.7854	0.6838	0.6368	0.6368	0.7575	0.6432	0.5829	0.6997	0.7962

Table 2 The diagnostic performance of our slice-selection method with TH_{slice_stiff} = 15 and at the 25^{th} percentile using different threshold value for classifying the tumors.

Threshold	True positives	False positives	True negatives	False negatives	Accuracy (%)	Sensitivity (%)	Specificity (%)
0.075	33	26	19	2	65	94.29	42.22
0.125	32	22	23	3	68.75	91.43	51.11
0.175	32	20	25	3	71.25	91.43	55.56
0.225	29	19	26	6	68.75	82.86	57.78
0.275	29	17	28	6	71.25	82.86	62.22

Table 3 Feature statistics of benign and malignant tumors in slices selected using our proposed method with TH_{slice_stiff} = 15 and at the 25th percentile.

Features		Benign		Malignant		*p*-value
		Mean ± SD	Median	Mean ± SD	Median	
Stiffness ratio (thresholding)	$stiff_5$		0.11		0.28	0.0026
	$stiff_{10}$		0.15		0.39	0.0067
	$stiff_{15}$	0.32 ± 0.26		0.47 ± 0.26		0.0130
	$stiff_{20}$	0.38 ± 0.27		0.53 ± 0.26		0.0130
	$stiff_{25}$	0.44 ± 0.28		0.59 ± 0.26		0.0210
	$stiff_{30}$	0.51 ± 0.29		0.64 ± 0.26		0.0340
	$stiff_{40}$		0.63		0.77	0.0606
	$stiff_{50}$		0.75		0.86	0.0720
Stiffness_ratio (FCM)	*fcm2_ratio*	0.66 ± 0.14		0.70 ± 0.12		0.1090
	fcm3_ratio	0.47 ± 0.15		0.54 ± 0.14		0.0280
Stiffness_mean	*fcm2_stiffmean*		21.89		13.82	0.0087
	fcm3_stiffmean		15.58		8.14	0.0058
Center_box	avg_box_{20}		30.23		14.31	0.0056
	avg_box_{30}		33.28		14.07	0.0061
Tumor boundary elasticity	*inner_mean*		60.92		51.99	0.0943
	outer_mean		69.36		65.35	0.1196
	diff_bands		9.71		9.28	0.5253
	tumor_mean	170.10 ± 41.34		147.43 ± 37.10		0.0130
Outside-tumor elasticity	*avg_outer_L*		49.28		42.98	0.2504
	avg_outer_R		52.34		36.72	0.1856
	avg_outer_U		50.04		22.10	0.0029
	avg_outer_D	59.00 ± 33.75		59.79 ± 34.39		0.9190
	avg_outer_UL		40.33		27.68	0.0182
	avg_outer_UR		44.16		24.39	0.0071
	avg_outer_LL	59.00 ± 38.98		58.99 ± 32.02		0.9990
	avg_outer_LR		45.78		49.80	0.9035
	min_outer		34.82		22.10	0.0817
	avg_outer		49.50		43.98	0.1128
Inside-tumor elasticity	*avg_inner_UL*		33.80		16.27	0.0087
	avg_inner_UR		24.41		9.14	0.0095
	avg_inner_LL		39.55		16.60	0.0690
	avg_inner_LR		34.65		20.89	0.0661
	avg_inner_C		35.17		12.18	0.0037
	min_inner		17.30		6.36	0.0085
	avg_inner		36.27		19.67	0.0100

Table 4 Feature statistics of benign and malignant tumors in physician-selected slices.

Features		Benign		Malignant		*p*-value
		Mean ± SD	Median	Mean ± SD	Median	
Stiffness ratio (thresholding)	$sitff_5$		0.18		0.38	0.0011
	$sitff_{10}$	0.28 ± 0.23		0.47 ± 0.28		0.0010
	$sitff_{15}$		0.37		0.60	0.0032
	$sitff_{20}$		0.43		0.65	0.0030
	$sitff_{25}$		0.49		0.72	0.0045
	$sitff_{30}$		0.55		0.75	0.0063
	$sitff_{40}$		0.68		0.81	0.0118
	$stiff_{50}$		0.79		0.88	0.0226
Stiffness_ratio (FCM)	*fcm2_ratio*	0.66 ± 0.12		0.74 ± 0.12		0.0090
	fcm3_ratio		0.50		0.56	0.0014
Stiffness_mean	*fcm2_stiffmean*		18.36		10.39	0.0042
	fcm3_stiffmean		9.92		6.78	0.0038
Center_box	avg_box_{20}		24.15		11.25	0.0027
	avg_box_{30}		27.19		13.45	0.0024
Tumor boundary elasticity	*inner_mean*		61.67		51.82	0.0325
	outer_mean	75.00 ± 23.18		61.72 ± 23.96		0.0140
	diff_bands		10.87		7.45	0.0473
	tumor_mean		50.51		36.12	0.0022
Outside-tumor elasticity	*avg_outer_L*	54.76 ± 27.54		38.93 ± 27.97		0.0130
	avg_outer_R	56.33 ± 31.46		43.42 ± 28.24		0.0610
	avg_outer_U		49.70		22.48	0.0027
	avg_outer_D		60.09		44.39	0.2585
	avg_outer_UL		46.37		21.79	0.0014
	avg_outer_UR		46.27		22.49	0.0151
	avg_outer_LL	58.25 ± 35.57		47.35 ± 29.45		0.1470
	avg_outer_LR		46.81		44.48	0.3297
	min_outer		32.71		14.78	0.0048
	avg_outer	55.44 ± 25.79		41.03 ± 26.35		0.0160
Inside-tumor elasticity	*avg_inner_UL*		27.91		11.67	0.0038
	avg_inner_UR		19.44		8.22	0.0143
	avg_inner_LL		35.60		15.80	0.0197
	avg_inner_LR		31.76		21.97	0.0168
	avg_inner_C		28.50		12.02	0.0015
	min_inner		11.96		4.66	0.0050
	avg_inner		28.63		12.37	0.0046

4.3 Tumor classification

In this experiment, in order to select the most useful elastographic features for classifying the breast tumors, the features with the *p*-value less than 0.05 are selected at first. The features of slice-selection method and physician-selected slice are selected in the beginning, respectively. Then, the backward feature elimination [28] is applied to eliminate the less important features with only slightly reducing the diagnostic performance to obtain the most appropriate features to diagnose the tumor, as listed in Table 5. Furthermore, the diagnostic performances of the binary logistic regression model for the selected most appropriate features by means of utilizing the leave-one-out cross-validation method on the slice-selection method and physician-selected slice are listed in Table 6, respectively.

In order to compare the outcomes of the selected most appropriate features on the two different schemes, the *p*-values of five performance indexes by the chi-square test and the Az values of the ROC curves by the z-test [30] are listed in Table 6. Moreover, the sensitivity and accuracy of our proposed slice-selection method are better than that of physician-selected slice and the specificity is similar on these two different representative slices. In addition, The ROC curves for diagnosing tumor using selected appropriate features based on our system-selected slice and physician-selected slice are shown in Fig. 13. Finally, some experiment examples of true positive (TP), true negative (TN), false negative (FN), and false positive (FP) cases are illustrated in Fig. 14-Fig. 17.

Table 5 The remaining features after applying the backward feature elimination on features with p-value < 0.05.

Slice-selected method	Features
System selection (11)	*$stiff_5$, $stiff_{15}$, $stiff_{20}$, $stiff_{30}$, fcm3_ratio, fcm2_stiffmean, fcm3_stiffmean, avg_box_{30}, tumor_mean, avg_inner_C, avg_inner*
Physician selection (19)	*$stiff_5$, $stiff_{15}$, $stiff_{40}$, fcm2_ratio, fcm3_stiffmean, avg_box_{20}, avg_box_{30}, outer_mean, diff_mean, tumor_mean, avg_outer_L, min_outer, avg_outer_UL, avg_outer_UR, avg_inner_UR, avg_inner_LL, avg_inner_LR, avg_inner_C, avg_inner*

Table 6 The performance indexes and p-values of performance indexes using chi-square test and Az value of ROC curve using z-test for the system-selected slice and physician-selected slice.

	Performance		p-value
	System-selection	Physician-selection	
Az	0.8014	0.7595	0.5955
Accuracy	71.25%	65.00%	0.3963
Sensitivity	91.43%	77.14%	0.1006
Specificity	55.56%	55.56%	1.0000
Positive predictive value	61.54%	57.45%	0.6787
Negative predictive value	89.29%	75.76%	0.1708

Note:

Accuracy = (TP+TN) / (TP+TN+FP+FN)

Sensitivity = TP / (TP+FN)

Specificity = TN / (TN+FP)

Positive Predictive Value = TP / (TP+FP)

Negative Predictive Value = TN / (TN+FN)

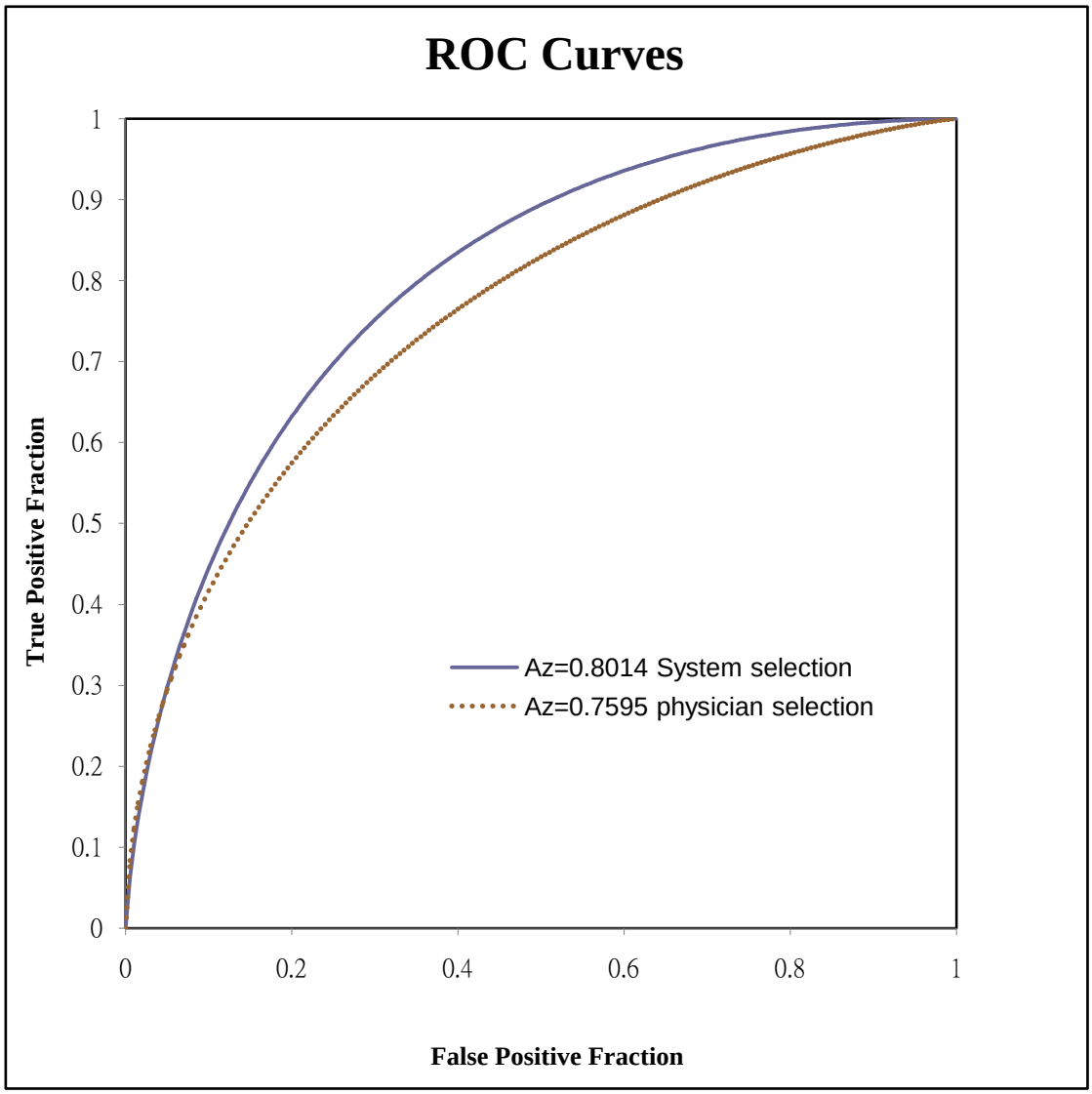

Fig. 13 The ROC curves for the system-selected slice and physician-selected slice.

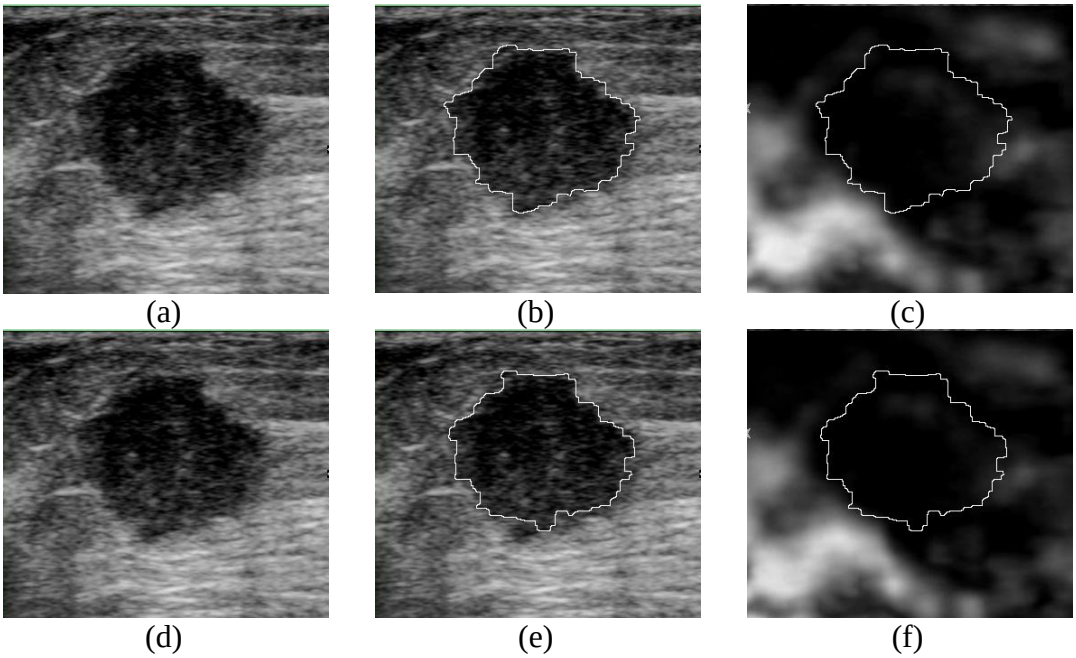

Fig. 14 A true positive example of invasive ductal carcinoma (a) The original image and (b)(c) the B-mode image and elastographic image with the segmentation result on the slice 23 selected by the proposed slice selection method. (d) The original image and (e)(f) the B-mode image and elastographic image with the segmentation result on the physician-selected image.

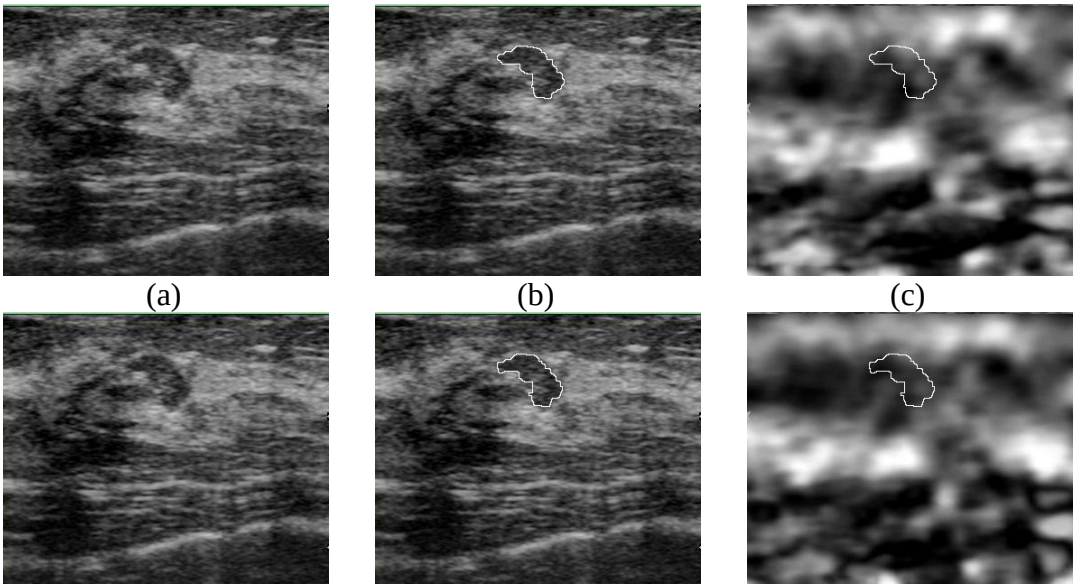

Fig. 15 A true negative example of epithelial hyperplasia (a) The original image and (b)(c) the B-mode image and elastographic image with the segmentation result on the slice 8 selected by the proposed slice selection method. (d) The original image and (e)(f) the B-mode image and elastographic image with the segmentation result on the physician-selected image.

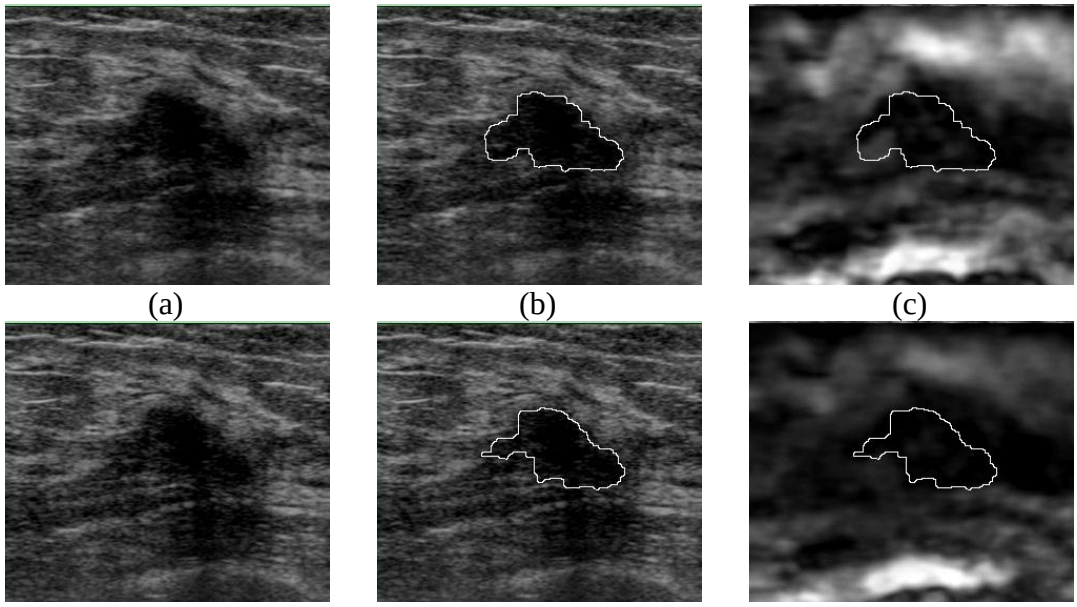

Fig. 16 A false positive example of fibrocystic change (a) The original image and (b)(c) the B-mode image and elastographic image with the segmentation result on the slice 108 selected by the proposed slice selection method. (d) The original image and (e)(f) the B-mode image and elastographic image with the segmentation result on the physician-selected image.

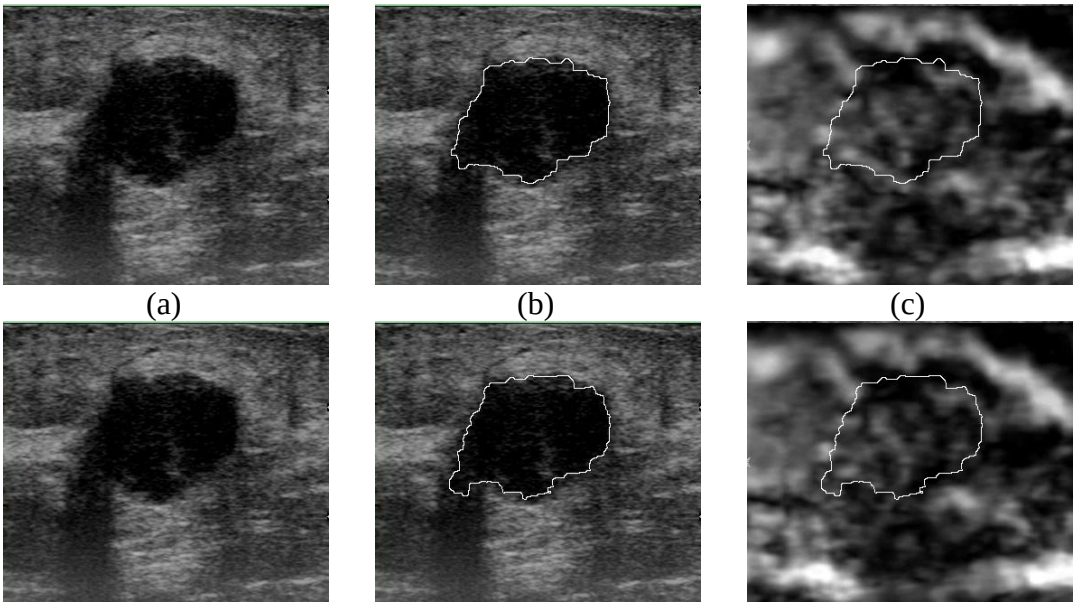

Fig. 17 A false negative example of invasive ductal carcinoma (a) The original image and (b)(c) the B-mode image and elastographic image with the segmentation result on the slice 38 selected by the proposed slice selection method. (d) The original image and (e)(f) the B-mode image and elastographic image with the segmentation result on the physician-selected image.

4.4 Discussion

According to Table 1, the representative slice selected by applying the slice-selection method on the whole slice is more appropriate as the TH_{slice_stiff} is set to 15 and at the 25^{th} percentile of sorted stiffness ratio, meaning the distribution of stiff tissues will not occupy too many areas in the whole image. It is reasonable that the slice might be over-compressed when there are too many stiff areas. From observing the Az values listed in Table 1, the better performance the slice at the more posterior percentile performs as the TH_{slice_stiff} increasing from 20 to 30 was applied on the whole slice. As

for selecting slice according to elasticity information within tumor regions, the slice at anterior percentile always performs best when $TH_{slice\_stiff} \geqq 20$. For selecting slice on the tumor region, the performance is also acceptable at the 75^{th} percentile with $TH_{slice\_stiff} = 15$ and at the 25^{th} percentile with $TH_{slice\_stiff} = 30$. However, the main drawback of this method is that its performance depends on the segmentation result. In [31], Chang et al. proposed two schemes to select slices based on SNR and CNR information, but the tumor contour must be found at first. However, our proposed method selected slices according to strain information of tissues in the whole slice with no needs to set up initial seeds for segmenting tumors. Therefore our scheme benefits from saving time for slice selection and avoiding using incorrect elasticity information within wrongly segmented tumor.

As mentioned before, the elastographic features are devided into five classes: stiffness ratio, average intensity of center box, tumor boundary elasticity, outside-tumor elasticity, and inside-tumor elasticity for comparing their performances. Table 7 listed the remaining features of each class calculated in system-selected slice after applying backward feature elimination. Similarly, the finally used features of each class calculated in physician-selected slice were listed in Table 8. For analyzing which class are the most useful in diagnosing, we adopted ROC analysis on features belonging to those five classes. Fig. 18 and Fig. 19 were the ROC curves of features belonging to the five classes on the system-selected and the physician-selected slice, respectively. We could conclude that features in class “stiffness_ratio” are most helpful in diagnosing since the Az value was highest in both figures.

From Table 6, the sensitivity of our proposed method was superior to that of the ground truth done by physicians, and other performance measures were similar to or better than those of the physician-selected slice. Although their performance is not

statistically significant in the current experiment, the physician will still benefit from the proposed slice selection method to reduce the time of selecting an appropriate representative slice.

In addition, we could compare our proposed method with the diagnosis result of Regner et al. [1] using the elastographic images captured by the same machine. In their study, the features, such as width and area ratios, are manually evaluated by five observers and the results of five observers were combined to acquire the final diagnosis performance. The sensitivity and specificity of our proposed method are 94.49% and 42.22% with the classification threshold 0.075 in Table 2, whereas those of the study of Regner et al. are 96% and 24%. The sensitivities of these two different schemes were similar but the specificity of our proposed method was better than that of their study.

Moreover, our proposed method automatically selected slices in terms of the elasticity information of tissues without letting the operator to spend the time for choosing the representative slice. Therefore, our approach could benefit from saving time for selecting an appropriate representative slice.

Table 7 The remaining features after applying the backward feature elimination on each class of the features with *p*-value < 0.05 for the system-selected slice in Table 3.

Feature classes	Features
Stiffness ratio	$stiff_5$, $stiff_{10}$, *fcm3_stiffmean*
Average intensity of center box	avg_box_{20}
Tumor boundary elasticity	*tumor_mean*
Outside-tumor elasticity	*avg_outer_UL, avg_outer_UR*
Inside-tumor elasticity	*avg_inner_C, avg_inner*

Table 8 The remaining features after applying the backward feature elimination on each class of the features with *p*-value < 0.05 for physician-selected slice in Table 4.

Feature classes	Features
Stiffness ratio	$stiff_{10}$, $stiff_{20}$, $stiff_{25}$, $stiff_{30}$, *fcm3_ratio*
Average intensity of center box	avg_box_{20}
Tumor boundary elasticity	*tumor_mean*
Outside-tumor elasticity	*avg_outer_L, avg_outer_UL*
Inside-tumor elasticity	*avg_inner*

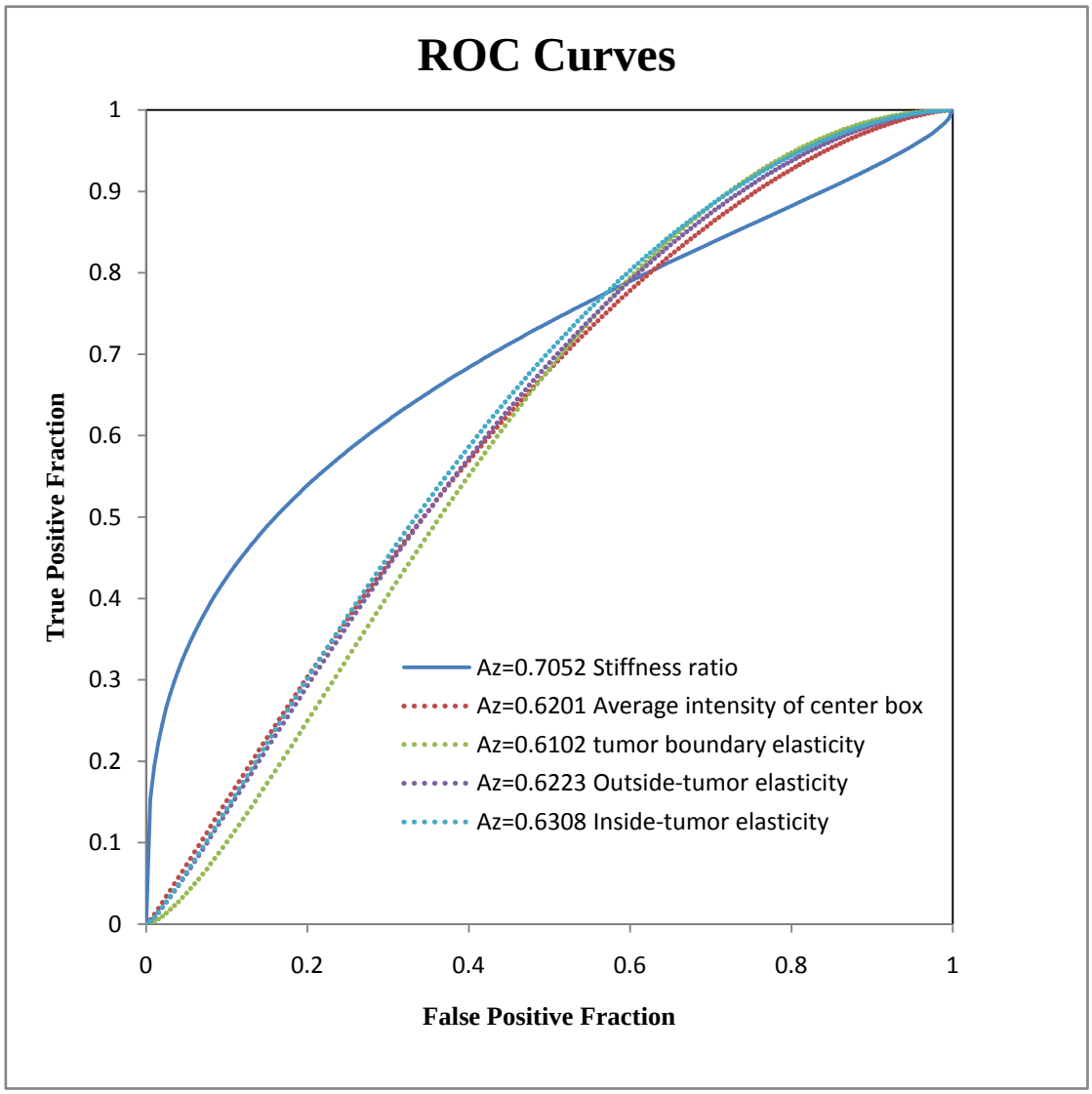

Fig. 18 The ROC curves for five different classes of the features on system-selected slice.

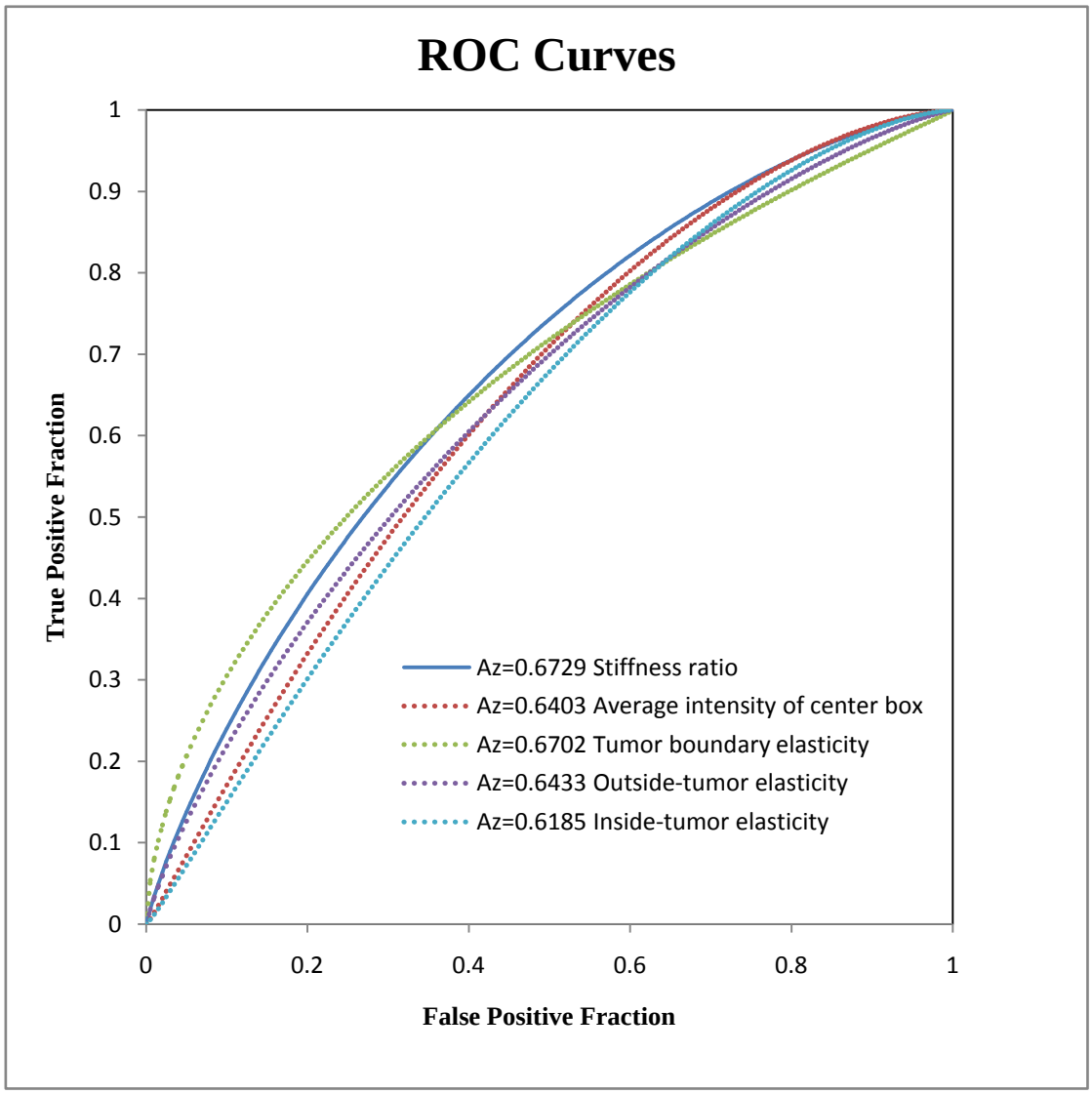

Fig. 19 The ROC curves for five different classes of the features on physician-selected slice.

Chapter 5

Conclusion and Future Works

The main purpose of this study is utilizing the elastographic features on the representative slice which is selected by the proposed slice-selection method from the dynamic elastographic video to diagnose the tumor. First, the slice-selection method was developed to select the representative slice instead of relying on the subjective perspective of the physician so as to diminishing the variability of observers. Next, in order to improve the consistency of the segmentation between the different operators, the contour of tumor delineated by the physicians is substituted with the automatic segmentation of the level set method. At last, the contour of tumor is applied to evaluate the elastographic features for the diagnosis of the breast tumor.

In the experiment, the diagnosis performances of accuracy, sensitivity, and specificity estimated by the leave-one-out method based on the elastographic features on the representative slice selected by the proposed slice-selection method are 71.25%, 91.43% and 55.56%, whereas 65.00%, 77.14% and 55.56% on the physician-selected slice. According to the experimental result, the performance of the proposed slice-selection method is similar with that done by the physician. Furthermore, the sensitivity and accuracy of proposed slice-selection method is better than physician-selected slice, and the specificity of these two different schemes is similar. Hence, the proposed slice-selection method could assist the physician in selecting the appropriate representative slice and decreasing the time of selection.

In the proposed method of segmentation, the automatic segmentation based on the level set method which delineates different contours of tumors by virtue of the inconsistent manipulation of inter-operator and difference of seeds will result in

different diagnostic performances changing with the different contours of tumors. Therefore, in order to obtain the better result of segmentation and reduce the variability of delineating the contour, the more robust and sophisticated automatic segmentation method is expected to be developed in the future. In addition, since the distribution of tissue strains (i.e. stiffness ratio mentioned before) could be used for the selection of the representative slice, stiffness ratios calculated using different TH_{slice_stiff} may be combined to select a more appropriate slice in the future. Moreover, the distribution of the soft tissue also could be combined as an additional reference. Furthermore, in order to reduce the effect of the some defective slices in the elasographic image and improve the accuracy of the diagnosis, the useful features, such as the shape, margin, and texture of the tumor on the B-mode image, could be also taken into account.

References

[1] D. M. Regner, *et al.*, "Breast lesions: evaluation with US strain imaging--clinical experience of multiple observers," *Radiology*, vol. 238, pp. 425-37, Feb 2006.

[2] T. J. Hall, *et al.*, "In vivo real-time freehand palpation imaging," *Ultrasound in Medicine and Biology*, vol. 29, pp. 427-35, Mar 2003.

[3] J. Ophir, *et al.*, "Elastography: a quantitative method for imaging the elasticity of biological tissues," *Ultrasonic Imaging*, vol. 13, pp. 111-34, Apr 1991.

[4] B. S. Garra, *et al.*, "Elastography of breast lesions: Initial clinical results," *Radiology*, vol. 202, pp. 79-86, Jan 1997.

[5] R. C. Booi, *et al.*, "Characterization of cysts using differential correlation coefficient values from two dimensional breast elastography: preliminary study," *Ultrasound in Medicine and Biology*, vol. 34, pp. 12-21, Jan 2008.

[6] N. Cho, *et al.*, "Nonpalpable breast masses: Evaluation by US elastography," *Korean Journal of Radiology*, vol. 9, pp. 111-118, 2008.

[7] Y. M. Sohn, *et al.*, "Sonographic Elastography Combined With Conventional Sonography How Much Is It Helpful for Diagnostic Performance?," *Journal of Ultrasound in Medicine*, vol. 28, pp. 413-420, 2009.

[8] A. Itoh, *et al.*, "Breast disease: Clinical application of US elastography for diagnosis," *Radiology*, vol. 239, pp. 341-350, May 2006.

[9] S. Raza, *et al.*, "Using Real-time Tissue Elastography for Breast Lesion Evaluation Our Initial Experience," *Journal of Ultrasound in Medicine*, vol. 29, pp. 551-563, 2010.

[10] A. Thomas, *et al.*, "Real-time elastography - an advanced method of ultrasound: first results in 108 patients with breast lesions," *Ultrasound in Obstetrics & Gynecology*, vol. 28, pp. 335-340, Sep 2006.

[11] H. Zhi, *et al.*, "Comparison of ultrasound elastography, mammography, and sonography in the diagnosis of solid breast lesions," *Journal of Ultrasound in Medicine*, vol. 26, pp. 807-815, 2007.

[12] Q. L. Zhu, *et al.*, "Real-time ultrasound elastography: Its potential role in assessment of breast lesions," *Ultrasound in Medicine and Biology*, vol. 34, pp. 1232-1238, 2008.

[13] A. Thomas, *et al.*, "Tissue Doppler and strain imaging for evaluating tissue elasticity of breast lesions," *Academic Radiology*, vol. 14, pp. 522-529, 2007.

[14] W. K. Moon, *et al.*, "Analysis of elastographic and B-mode features at

sonoelastography for breast tumor classification," *Ultrasound in Medicine and Biology*, vol. 35, pp. 1794-802, Nov 2009.

[15] J. M. Chang, *et al.*, "Breast mass evaluation: factors influencing the quality of US elastography," *Radiology*, vol. 259, pp. 59-64, Apr 2011.

[16] W. K. Moon, *et al.*, "Breast tumor classification using fuzzy clustering for breast elastography," *Ultrasound in Medicine and Biology*, vol. 37, pp. 700-8, May 2011.

[17] R. Malladi, *et al.*, "Shape Modeling with Front Propagation - a Level Set Approach," *IEEE Transactions on Pattern Analysis and Machine Intelligence*, vol. 17, pp. 158-175, Feb 1995.

[18] S. Osher and J. A. Sethian, "Fronts Propagating with Curvature-Dependent Speed - Algorithms Based on Hamilton-Jacobi Formulations," *Journal of Computational Physics*, vol. 79, pp. 12-49, Nov 1988.

[19] J. S. Suri, *Advances in diagnostic and therapeutic ultrasound imaging*. Boston ; London: Artech House, 2008.

[20] R. Deriche, "Fast Algorithms for Low-Level Vision," *IEEE Transactions on Pattern Analysis and Machine Intelligence*, vol. 12, pp. 78-87, Jan 1990.

[21] J. Serra, "Biomedical Image Analysis by Mathematical Morphology," *Pathologie Biologie*, vol. 27, pp. 205-207, 1979.

[22] S. R. Sternberg, "Grayscale Morphology," *Computer Vision Graphics and Image Processing*, vol. 35, pp. 333-355, Sep 1986.

[23] H. J. A. M. Heijmans, "Theoretical Aspects of Gray-Level Morphology," *IEEE Transactions on Pattern Analysis and Machine Intelligence*, vol. 13, pp. 568-582, Jun 1991.

[24] R. C. Gonzalez, *et al.*, *Digital image processing*, third ed. Upper Saddle River, New Jersey: Pearson Prentice Hall, 2009.

[25] J. A. Sethian, "Numerical Algorithms for Propagating Interfaces - Hamilton-Jacobi Equations and Conservation-Laws," *Journal of Differential Geometry*, vol. 31, pp. 131-161, Jan 1990.

[26] J. C. Bezdek, *Pattern Recognition With Fuzzy Objective Function Algorithms*: New York: Plenum, 1981.

[27] D. W. Hosmer and S. Lemeshow, *Applied logistic regression*, 2nd ed. New York: Wiley, 2000.

[28] W. C. Shen, *et al.*, "Breast ultrasound computer-aided diagnosis using BI-RADS features," *Academic Radiology*, vol. 14, pp. 928-939, Aug 2007.

[29] E. Alpaydin, *Introduction to machine learning*. Cambridge, Mass.: MIT Press, 2004.

[30] A. P. Field, *Discovering statistics using SPSS*, 3rd ed. Los Angeles: SAGE

Publications, 2009.

[31] Y. C. Chang, *et al.*, "Automatic selection of representative slice from cine-loops of real-time sonoelastography for classifying solid breast masses," *Ultrasound Med Biol*, vol. 37, pp. 709-18, May 2011.